JOURNAL OF CHEMICAL INFORMATION AND MODELING

Article

pubs.acs.org/jcim

Structural Basis for the Mutation-Induced Dysfunction of Human CYP2J2: A Computational Study

Shan Cong,[†,‡] Xiao-Tu Ma,[†] Yi-Xue Li,*[,‡,§,∥] and Jing-Fang Wang*[,∥]

[†]Key Laboratory of Systems Biomedicine (Ministry of Education), Shanghai Center for Systems Biomedicine, Shanghai Jiao Tong University, Shanghai 200240, China

Supporting Information

ABSTRACT: Arachidonic acid is an essential fatty acid in cells, acting as a key inflammatory intermediate in inflammatory reactions. In cardiac tissues, CYP2J2 can adopt arachidonic acid as a major substrate to produce epoxyeicosatrienoic acids (EETs), which can protect endothelial cells from ischemic or hypoxic injuries and have been implicated in the pathogenesis of coronary artery disease and hypertension. However, some CYP2J2 polymorphisms, i.e., T143A and N404Y, significantly reduce the metabolism of arachidonic acid. Lacking experimental structural data for CYP2J2, the detailed mechanism for the mutation-induced dysfunction in the metabolism of arachidonic acid is still unknown. In the current study, three-dimensional structural models of the wild-type CYP2J2 and two mutants (T143A and N404Y) were constructed by a coordinate reconstruction approach and ab initio modeling using CYP2R1 as a template. The structural analysis of the computational models showed that the wild-type CYP2J2 exhibited a typical CYP fold with 12 alpha-helices and three beta-sheets on one side and with the heme group buried deeply inside the core. Due to the small and hydrophobic side-chain, T143A mutation could destabilize the C helix, further placing the water access channel in a closed state to prevent the escape of the produced water molecules during the catalytic processes. N404Y mutation could reposition the side-chain of Leu[378], making it no longer form a hydrogen bond with the carboxyl group of arachidonic acid. However, this hydrogen bond was essential for substrate recognition and positioning in a correct orientation.

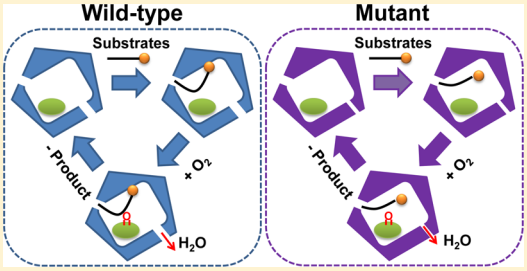

INTRODUCTION

Arachidonic acid (officially named 5,8,11,14-eicosatetraenoic acid) is a polyunsaturated omega-6 fatty acid and is believed to be an essential fatty acid synthesized from linoleic acid or directly obtained from diet.[1] In the body's cells, Arachidonic acid is stored within the phospholipids of cell membranes, especially phosphatidylethanolamine, phosphatidylcholine, and phosphatidylinositides, and is abundant in the brain, muscles, and liver.[2] As a precursor of the eicosanoids, arachidonic acid has been a key inflammatory intermediate, playing crucial roles in physiology and pathophysiology in inflammatory reactions.[3] Arachidonic acid can be metabolized into both pro-inflammatory and anti-inflammatory molecules,[4] but the increased free arachidonic acid levels can reduce pro-inflammatory IL-6 and IL-1 levels and increase anti-inflammatory tumor necrosis factor-beta.[5] Thus, how arachidonic acid is metabolized in the body will directly influence its inflammatory or anti-inflammatory activities.

In the liver, arachidonic acid is mainly metabolized by the cytochrome P450 (CYP) 2J subfamily, to produce isoform-specific sets of regio- and stereoisomeric epoxyeicosatrienoic acids (EETs, Figure S1).[6] EETs are second messengers of a number of hormones and growth factors with key roles in the regulation of vascular renal and cardiac function.[7,8] These arachidonic acid metabolites are also major endothelium-derived hyperpolarizing factors (EDHF) in the vascular beds and are involved in an antihypertensive and organ-protective mechanism by activating endothelial nitric oxide synthase,[9] or by modulating other agonist-induced mechanisms in endothelial cells.[10] Additional evidence show that EETs are also able to mediate anti-inflammatory and antiapoptotic mechanisms to protect against cell and organ injury,[11] and to serve as regulators in vascular healing and in prevention of uncontrolled vascular remodeling.[12] According to the animal models and initial human studies, the alterations in the CYP-mediate arachidonic acid metabolism are associated with the development of hypertension and target organ damage.[13−15]

Human CYP2J2 is the only CYP enzyme expressed in the cardiovascular system.[16] This CYP enzyme is able to catalyze many reactions involved in drug metabolism and synthesis of cholesterol, steroids, and other lipids. Of most importance, CYP2J2 can adopt arachidonic acid as a major substrate in cardiac tissues and produces 5,6-, 8,9-, 11,12-, and 14,15-EETs in a ratio of ∼37:18:24:21.[16] As mentioned above, these arachidonic acid metabolites can protect endothelial cells from ischemic or hypoxic injuries. So, CYP2J2 and EETs have been implicated in the pathogenesis of coronary artery disease and hypertension.[17] For different individuals, CYP2J2 shows some significant polymorphisms, i.e., T143A and N404Y.[18] T143A

Received: January 10, 2013

   dx.doi.org/10.1021/ci400003p | J. Chem. Inf. Model. XXXX, XXX, XXX−XXX

can significantly reduce the metabolism reaction of arachidonic acid, exhibiting only 59% of the wild-type CYP2J2 activity. N404Y is essentially inactive in the arachidonic acid mechanism, showing only 5% of the wild-type CYP2J2 activity.

By now, the detailed mechanism for such mutation-induced dysfunction in arachidonic acid metabolism mentioned above is still unclear. In the present study, we attempted to employ molecular modeling and simulation to study the metabolic mode of arachidonic acid in human CYP2J2, with the aim of providing structural insights into the dysfunction mechanism.

MATERIALS AND METHODS

1. Constructing Structural Models of Human CYP2J2. As there is no experimental structural data available in the protein structure databases (i.e., RCSB Protein Data Bank), we had to predict the three-dimensional structural model for human CYP2J2. The original sequence of the wild-type CYP2J2 was extracted from the UniProt Database (www.uniprot.org), a comprehensive resource for protein sequence and annotation data, with an accession number of P51589. The original sequence was subsequently submitted to RCSB Protein Data Bank (PDB) to search for a structural template, and the crystal structure of CYP2R1 (PDB ID 3c6g.pdb) was finally picked up for the further model construction.[19] This crystal structure was first released in 2008 with a resolution of 2.80 Å,[19] and the sequence identity between this crystal structure and CYP2J2 was 42.7% (also see the sequence alignment shown in Figure S2).

On the basis of the atomic coordinates of the crystal structure of CYP2R1 and the sequence alignment shown in Figure S2, the three-dimensional structural model of the wild-type CYP2J2 for the aligned regions with the template structure was modeled by the segment matching or coordinate reconstruction approach.[20,21] This approach has been successfully used to predict many essential proteins or enzymes (i.e., xylose reductase,[22] M2 proton channel,[23] NDM-1,[24] and other CYP enzymes[25,26]) before their crystal structures were available, providing timely useful information for studying the protein structure−function relationship and drug development.[27,28] The unaligned regions with the template structure were then constructed using an ab initio modeling approach.[29] Using similar methods, the structural models of both T143A and N404Y mutants were built.

2. Generating Arachidonic Acid Binding Mode. The three-dimensional structural models for the wild-type and mutated CYP2J2 enzymes mentioned above were subjected to a short time molecular dynamics simulation (∼1 ns), on the basis of which 1000 conformations for each enzyme were generated. For each conformation, flexible docking procedures were employed with Monte Carlo simulated annealing by the docking module in MOE 2008.[30] During the flexible docking processes, the docking program generated a diversified group of conformations by making random changes of the coordinates of arachidonic acid. Once a new conformation of arachidonic acid was generated, the searching for the favorable binding modes was performed within a specified docking box, using Monte Carlo simulated annealing to optimize the purely spatial contacts and electrostatic interactions. The best 100 binding modes for each conformation were selected using the London dG scoring function,[30] and all the binding modes were clustered and revalidated to pick up the final binding mode of arachidonic acid for the wild-type and mutated CYP2J2 enzymes.

3. Molecular Dynamics Simulation. The final binding modes of arachidonic acid for the wild-type and mutated CYP2J2 enzymes were employed as initial structures for the further molecular dynamics (MD) simulations. Except for the polar hydrogen and heavy atoms, all the other atoms (including nonpolar hydrogen atoms) in the simulation systems were removed. The pK_a values for each residue in the CYP2J2 structure were computed by Delphi as a Poisson−Boltzmann solver with a dielectric constant of 4.0.[31] Hydrogen atoms were then added to the CYP2J2 structure with the t-Leap procedure implemented in the AMBER 10.0 package based on the computational pK_a values, to give a total charge of +5.0. The simulation systems were then solvated in a simulation box with ∼18 000 explicit TIP3P water molecules. To neutralize the simulation systems, five chloride ions were added to randomly replace five water molecules in the simulation box. The atoms of the wild-type and mutant CYP2J2 structures were parametrized by AMBER force field parameters,[32] while the force field parameters of the protoporphyrineIX group in the CYP2J2 structure were obtained from previous QM/MM simulations.[33] The force field parameters of arachidonic acid were generated by the Antechamber module implemented in the AMBER 10.0 package.

After solvation, all the simulation systems were subjected to steepest descent energy minimization (∼5000 steps), followed by a conjugate gradient for the next 5000 steps. All the systems were then equilibrated with the heavy atoms of the protein, heme, and arachidonic acid fixed by a short-time MD simulation (∼ 1 ns) to reduce the van der Waals conflicts. Finally, 10-ns MD simulations were performed for each simulation system at normal temperature (310 K) using the AMBER 10.0 package with periodic boundary conditions and the NPT ensemble.[34] The weak-coupling algorithm[35] was used to maintain the NPT ensemble. To maintain the simulation systems at a constant temperature and pressure, the Berdensen thermostat was applied with a coupling time of 0.1 and 1.0 ps.The SHAKE algorithm was applied to constrain all the chemical bonds,[36] and atom velocities for start-up runs were obtained according to the Maxwell distribution at 310 K.[37] For each system, 10 independent runs with different start-up runs were performed. The isothermal compressibility was set to 4.5 × 10^{-5} bar for solvent simulations. The electrostatic interactions were treated by the PME algorithm with an interpolation order of 4.0 and a grid spacing of 0.12 nm.[38] The van der Waals interactions were calculated using a cutoff of 12 Å.[39] All the simulations were performed with a time step of 2 fs, and the coordinates for all the systems were saved every 1 ps.

4. Binding Free Energy Estimation. The binding free energies of the arachidonic acid with both wild-type and mutant structures can be dissected into the following terms:

$$\Delta G_{\text{binding}} = \Delta G_0 + \Delta G_{\text{vdw}} + \Delta G_{\text{Hbond}} + \Delta G_{\text{deformation}} + \Delta G_{\text{hydrophobic}} \quad (1)$$

where ΔG_0 is the regression constant including translational and rational entropy loss effects, ΔG_{vdw} accounts for the van der Waals interactions between the arachidonic acid and the CYP2J2 structure, ΔG_{Hbond} accounts for the hydrogen bonding between the arachidonic acid and the CYP2J2 structure, and $\Delta G_{\text{deformation}}$ and $\Delta G_{\text{hydrophobic}}$ account for the deformation and the hydrophobic effects between the arachidonic acid and the CYP2J2 structure, respectively. According to the standard thermodynamic relation[40,41]

dx.doi.org/10.1021/ci400003p | J. Chem. Inf. Model. XXXX, XXX, XXX−XXX

$$\Delta G_{binding} = RT \ln(K_i) \quad (2)$$

where R, T, and K_i are the universal gas constant, thermodynamic temperature, and dissociation equilibrium constant, respectively, we can estimate the binding free energies from calculating the dissociation equilibrium constant K_i, which was treated as an average of three empirical scoring functions:[42]

$$pK_i = (pK_{HP} + pK_{HS} + pK_{HM})/3 \quad (3)$$

$$pK_{HP} = 3.441 + 0.004 \times VDW + 0.054 \times HB + 0.009 \times HP - 0.061 \times RT \quad (4)$$

$$pK_{HS} = 3.328 + 0.004 \times VDW + 0.073 \times HB + 0.004 \times HS - 0.090 \times RT \quad (5)$$

$$pK_{HM} = 3.567 + 0.004 \times VDW + 0.101 \times HB + 0.387 \times HM - 0.097 \times RT \quad (6)$$

where VDW, HB, and RT stand for the van der Waals interaction, hydrogen bonding interaction, and deformation effects, respectively. For different empirical scoring functions, the hydrophobic effects were calculated by different algorithms: pK_{HP} uses the hydrophobic contact algorithm, in which the hydrophobic effects are estimated by summing up the hydrophobic atom pairs formed between the arachidonic acid and the CYP2J2 structure. pK_{HS} employs the hydrophobic surface algorithm, where the hydrophobic effects are assumed to be proportional to the buried hydrophobic surfaces of the arachidonic acid. pK_{HM} adopts the hydrophobic matching algorithm, in which different parts of the arachidonic acid sense the protein differently due to the heterogeneous nature of the binding site.

RESULTS AND DISCUSSION

1. Three-Dimensional Structural Models of CYP2J2. As expected, the three-dimensional structural model of the wild-type CYP2J2 exhibited a typical CYP folding structure:[43] 12 alpha-helices (designated from A to L) and three beta-sheets (designated from β1 to β3) on one side of the structural model with the heme group buried deeply inside the core of the structural model (Figure 1). According to the sequence analysis of human CYP enzymes, the wild-type CYP2J2 exhibited comparatively high sequence similarities with CYP2R1 (42.7%), CYP2A6 (38%), and CYP2E1 (37%). So, the computational model of the wild-type CYP2J2 showed highly structural similarities with the CYP enzymes mentioned above.

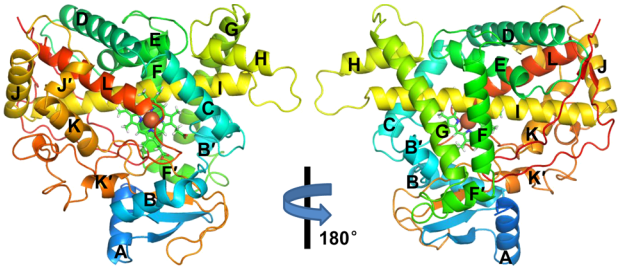

Figure 1. Schematic illustration of the three-dimensional structural model of the wild-type CYP2J2. The structural model of the wild-type CYP2J2 exhibits a typical CYP fold with 12 alpha-helices (designated A–L) and three beta-sheets (designated β1–β3) on one side of the structural model with the heme group buried deeply inside the core of the structural model. The backbone structure is rainbow colored from N terminus (blue) to C terminus (red).

Among the helices in the computational model of the wild-type CYP2J2, C, E, F, I, and L helices constituted the core region of the protein. These helices together with B′, F′, and K helices formed the active site pocket for the unsaturated fatty acid substrates, which were quite hydrophobic and much smaller than the other mammalian CYP enzymes. The volume of the active site pocket for the wild-type CYP2J2 was ~320 cubic angstroms, while that of CYP3A4 (which could adopt a wide range of substrates) was ~1500 cubic angstroms.[44−46] However, the volume of the active pocket of the wild-type CYP2J2 was quite similar to those of CYP2R1 and CYP2E1, which was also reported to be involved in the fatty acid metabolism.

The amino acid residues plotting out the active site cavity of the computational model included Ala^{311} and Thr^{315} on the successive turns of the I helix that belonged to the active site. The long I helix ran across the entire computational model, which was regarded to be essential for the delivery of a proton to an O_2 molecule during the CYP catalytic cycle.[47,48] The opposing face of the active site was formed by the intersection of the residues in and near the B′ helix (i.e., Arg^{117}, Ile^{127}, and Met^{128}), the loop between the K helix and β_{1-4} turn (i.e., Ile^{376} and Val^{380}), and the β_{4-1}/β_{4-2} turn (i.e., Ile^{487}).

For comparison, we also generated a CYP2J2 structural model using the web server LOMETS (Local Meta-Threading-Server),[49] which can predict protein structures by ranking and selecting models from eight state-of-the-art threading programs. The best LOMETS models were generated by the threading programs MUSTER, SP3, and SPARKS2 with a Z-score of 18.11. This model also showed a backbone RMS deviation of 1.18 Å from our model, giving an indication that the structural models generated by both methods were quite similar.

2. Validation and Verification of the Computational Models. To validate the computational models involved in the current study, multiple approaches were employed. First, to check the stereochemistry quality and structural feature, Procheck was employed to compare the geometry of the residues in a given protein structure with the stereochemical parameters derived from crystal or NMR structures.[50] The Procheck result of the computational structure showed that 87.4% of the residues were located in the most favorable region, 7.9% in the additional allowed region, 1.8% in the generously allowed region, and only 2.9% in the disallowed region (Table S1). For a good quality model, it is expected that the residues located in the most favorable and additional allowed regions should be more than 90%, which is the case for the computational structure of the wild-type CYP2J2. For the main-chain residues of our computational model, 98.2% of the bond lengths and 95.9% of the bond angles were within the allowed limitations. The Procheck results for the T143A and N404Y mutants are summarized in Table S1.

Second, to further check the global quality of the computational model, a scoring function QMEAN was used,[51] which is a linear combination of Cβ interaction energy, all-atom pairwise energy, solvation energy, torsion angle energy, secondary structure, and solvent accessibility. The QMEAN score, ranging between 0 and 1, with a higher value to reflect a better quality of the query model, for the model of the wild-type CYP2J2 was 0.63 (Figure S3A). Additionally, a Z-score was involved to compare the computational model with the

dx.doi.org/10.1021/ci400003p | J. Chem. Inf. Model. XXXX, XXX, XXX−XXX

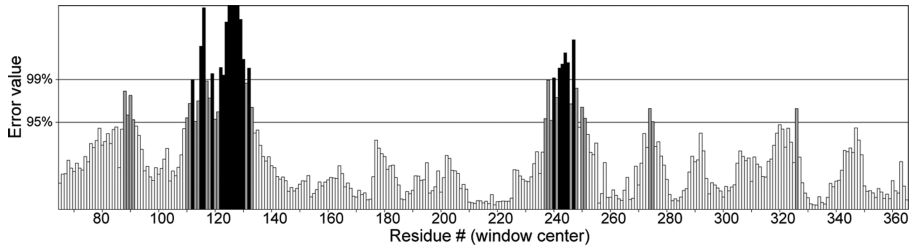

Figure 2. ERRAT error values for the computational structure of the wild-type CYP2J2. On the error axis, two lines are drawn to indicate the confidence with which it is possible to reject regions that exceed that error values. The overall quality factor, which is used to express the percentage of the protein for which calculated error value falls below the 95% rejection limit, of the current model is 78.34.

reference crystal structures of similar size, which is usually used to evaluate the absolute model quality (Figure S3B).

Third, the per residue errors for the computational model of the wild-type CYP2J2 were further checked by ERRAT,[52] which plotted the error values as a function of the position of a sliding nine-residue window (Figure 2). The ERRAT error function is based on the statistic information of nonbonded interactions between atoms in the query model in comparison with the crystal structures. The error values at more than the 95% confidence level mean that only 5% of the known proteins are expected to have an error value above this level. The ERRAT result reported an overall quality factor of 78.34, indicating that the error values of 78.34% residues were below the 95% rejection limitation. As shown in Figure 2, two regions (residues 110−132 and 240−247) were found to have error values more than 95% confidence level. These regions were mainly located on the flexible loops.

Finally, Verify3D was employed to analyze the compatibility of the computational model of the wild-type CYP2J2 with its amino acid sequence.[53] In this approach, each residue of the computational model was assigned a structural class based on its location and environment (alpha, beta, loop, polar, nonpolar, etc). A collection of good structures is used as a reference to obtain a score for each of the 20 amino acids in the structural class mentioned above. In the current case, Verify3D result showed that 90.97% of the residues in our computational model had an averaged 3D−1D score >0.2.

In sum, all the structural validation algorithms mentioned above have shown that the computational model of the wild-type CYP2J2 was indeed quite reliable and may be considered as a solid footing for further studies.

3. Arachidonic Acid Binding Mode and Interactions. On the basis of the computational model of the wild-type CYP2J2, the favorable binding mode of arachidonic acid was also obtained and shown in Figure 3. The RMS deviations of the protein backbone along the molecular dynamics trajectories (Figure S4) showed that the favorable binding modes in all the systems were equilibrated with the final RMS deviation values less than 2 Å. This observation also indicated that the mutations (T143A and N404Y) did not induce large-scale structural alterations for the entire protein structure. Additionally, the comparatively small RMS deviations of the arachidonic acid in the wild-type structure (Figure S5) also showed that the binding pose of the arachidonic acids was stable.

According to the crystal structure analysis of the CYP2 subfamily, six putative substrate recognition sites (designated SRS 1−6) for mammalian CYP enzymes have been proposed.[54] However, only five substrate recognition sites mentioned above were detected in arachidonic acid binding mode of CYP2J2. The loop between B′ and C helices was identified as the SRS1

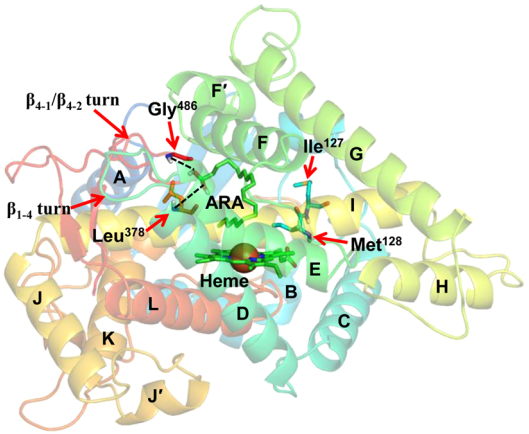

Figure 3. The favorable binding mode of arachidonic acid. In the favorable binding mode, the carboxyl group of arachidonic acid (ARA) was recognized and positioned by Gly[486] and Leu[378] using hydrogen bonding interactions. The aliphatic chain of ARA was stabilized by the hydrophobic interactions with the active site residues, i.e., Ile[127], Met[128], Ile[376], and Pro[381].

site in mammalian CYP enzymes, which was the case in the favorable binding mode of arachidonic acid. In the favorable binding mode of arachidonic acid, the corresponding region was a very long loop (residues 120−132) with the part near Leu[126], Ile[127], and Met[128] close to the heme group. In the favorable binding mode of arachidonic acid, this region (the loop near Leu[126], Ile[127], and Met[128]) could stabilize the aliphatic chain of the substrate by hydrophobic interactions.

The C-terminal region of the F helix and N-terminal region of the G helix were determined as SRS2 and SRS3 sites in mammalian CYP enzymes, respectively. In the favorable binding mode of arachidonic acid, the F helix was located on the protein surface and at the entrance of the substrate access channel (labeled as the S channel in Figure 4A). This helix together with the E helix, I helix, and the loop after the L helix, formed the substrate access channel. In the favorable binding mode of arachidonic acid, as in other CYP enzymes, the C-terminal region of the F helix acted as the SRS2 site to provide hydrophobic contacts with the substrate. However, the G helix in the computational model was far away from the substrate, and the traditional SRS3 site was thus not detected.

The central region of the I helix was identified as the SRS4 site in mammalian CYP enzymes. In the favorable binding mode of arachidonic acid, this helix (I helix) ran across the entire protein structure, playing an important role for the delivery of a proton to an O_2 molecule during the catalytic cycle. As the other CYP enzymes, the I helix in CYP2J2 was the SRS4 site, not only acting as a part of the active site but also a

dx.doi.org/10.1021/ci400003p | J. Chem. Inf. Model. XXXX, XXX, XXX−XXX

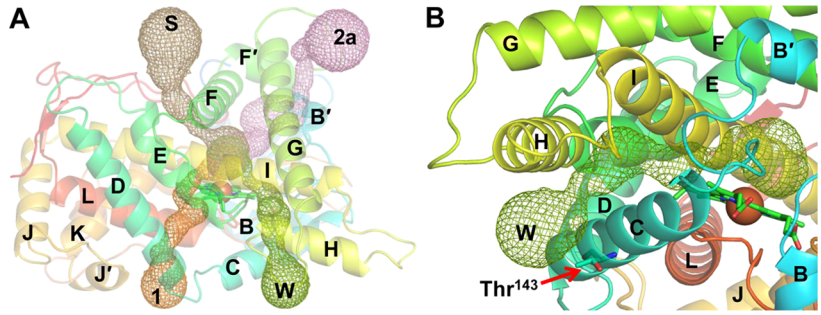

Figure 4. Illustration showing the access channels in the computational model of CYP2J2. (A) The substrate and water access channels in the computational model of the wild-type CYP2J2. The backbone structure of the computational model was rainbow colored from N terminus (blue) to C terminus (red). The substrate and water access channels were named S and W channels and are shown in mesh representations. (B) Close-view of the water access channel in the wild-type enzyme. The water access channel in CYP2J2 was composed of C, D, H, and I helices. The T143A mutation was located on the N-terminal region of the C helix, capable of destabilizing the C helix. The substrate and water access channels in this figure were identified by the Adaptive Poisson−Boltzmann Solver (APBS) implemented in PyMol 0.99.

key component of both substrate and water access channels (Figure 4A). This helix also had a significant impact on the active-site pocket volume. For instance, the active-site pocket volume of CYP3A4 was about 1500 cubic angstroms based on the crystal structure 1WE0. However, it could reach up to 3800 cubic angstroms in the apo CYP3A4 in the additional molecular dynamics simulations.[46]

The loop between the K helix and β_{1-4} turn was identified as the SRS5 site in mammalian CYP enzymes, which was also the case of the favorable binding mode of arachidonic acid. Similar to the SRS1 site, this region contained some important residues (i.e., Ile^{376} and Pro^{381}) that could provide hydrophobic contacts to stabilize the aliphatic chain of the substrate.

The region in the β_{4-1}/β_{4-2} turn was identified as the SRS6 site in both the mammalian CYP enzymes and the current case. In the favorable binding mode of arachidonic acid, this region contained two key residues Leu^{378} and Gly^{486} that formed two significant hydrogen bonds with the carboxyl group of arachidonic acid (Figure 3). When the substrate entered into the active site, the hydrogen bonds formed by Leu^{378} and Gly^{486} were able to specifically recognize the carboxyl head of the substrate, subsequently positioning the substrate in a correct orientation for the further catalytic processes. This region was also at the entrance of the substrate access channel, which could control the substrate access by its flexible motions.

4. Implications for T143A-Induced Enzyme Dysfunction. As reported by King and his co-workers,[18] the CYP2J2 variant with T143A mutation in Exon 3 (also known as the CYP2J2*2 polymorphism) showed a statistically significant decrease in enzyme activity, which was 59% of the wild-type CYP2J2. This mutation was located in the C helix far away from the active site pocket, and not in the putative SRS sites mentioned above. However, the C helix played a key role for substrate access and recognition in the active site. Although the T143A mutation was located on the N-terminal side of this helix, the C-terminal side of this helix was believed to act as the SRS2 site to provide hydrophobic contacts with the fatty acid substrates.

The substitution of alanine for threonine at amino acid position 143 was not propitious to stabilize the helical structure. This was mainly because the side-chain of alanine in the CYP2J2*2 polymorphism was too small to form steric effects or interact with other residues, which was essential for forming helical structures. As the C helix was located at the protein surface, the replacement of alanine at amino acid position 143 could make the side-chain of the residue at position 143 hydrophobic, which was hydrophilic in the wild-type CYP2J2. The hydrophobic side-chain was believed to be unstable in the water environments, further destabilizing the helical structures.

Additionally, the C helix was also an important component for the water access channel (labeled as W channel in Figure 4B) in CYP2J2. The entire water channel was composed of C, H, and I helices, among which the C and H helices formed the first gate of the water access channel. The second gate of the water access channel was constituted by the I helix as well as the loop region between the B′ and C helices. In the wild-type CYP2J2, the diameter of the narrowest part of the first gate was 6.65 ± 1.08 Å, while that in the T143A mutant was 3.87 ± 1.21 Å. As a comparison, the diameter of a water molecule is ∼4 Å. This finding indicated that the water access channel in the wild-type enzyme was in an open state, while it was closed in the T143A mutant. However, during the CYP catalytic processes, a water molecule could be released together with the final products.[55,56] This water molecule should escape from the active site by the water access channel mentioned above. The closed water access channel in the T143A mutant could prevent the escape of the produced water, causing the coemption of water molecules in the active site, which could shut down the proton transfer during the CYP catalytic processes.

5. Implications for N404Y-Induced Enzyme Dysfunctin. Different from the T143A mutant, the N404Y mutant (also known as CYP2J2*6) was essentially inactive in the arachidonic acid metabolism, with only 5% of the wild-type enzyme activity.[18] In the computational models of CYP2J2, this mutation (N404Y) was located on the loop near the N-terminal region of the K′ helix. The K′ helix was a short helix in CYP2J2, only constituted by six residues (Leu^{405}, Thr^{406}, Ala^{407}, Leu^{408}, His^{409}, and Arg^{410}). The loop between the K′ helix and L helix contained a conserved cysteine (Cys^{448}), functioning to ligate the heme group. As the N404Y mutation was not in the active site pocket of CYP2J2, it was expected that this mutation could not directly change the substrate binding in the active site. Indeed, the N404Y mutation impacted the substrate recognition and binding by an indirect approach. The substitution of tyrosine for asparagine at amino acid position 404 led to a comparatively large and aromatic side-chain. The steric effect of the Tyr^{404} side-chain could further reposition the side-chain of Leu^{378}, making it no longer form a hydrogen bond with the carboxyl group of arachidonic acid (Figure 5). This

dx.doi.org/10.1021/ci400003p | J. Chem. Inf. Model. XXXX, XXX, XXX−XXX

alteration would weaken the substrate binding affinity, so as to reduce the substrate specificity of CYP2J2.

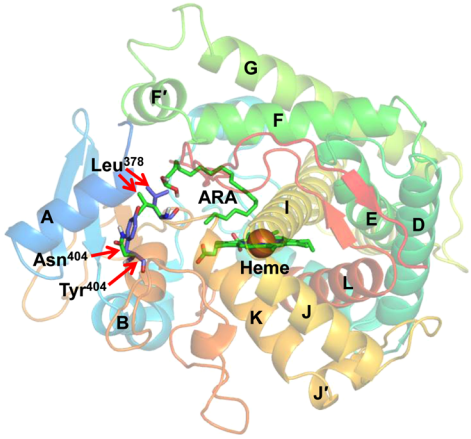

Figure 5. Comparison of the side-chain conformation of the wild-type CYP2J2 and N404Y mutant. The residues in the wild-type and N404Y mutant were mainly colored in green and purple, respectively. In the N404Y mutant, the substitution of tyrosine for asparagine at amino acid position 404 led to a comparatively large and aromatic side-chain, which could reposition the side-chain of Leu^{378}, making it no longer form a hydrogen bond with the carboxyl group of arachidonic acid.

This is also supported by the RMS deviations of the arachidonic acid (Figure S5). Compared with the wild-type structure, the RMS deviations of the arachidonic acid in the N404Y mutant structure were more fluctutated, indicating that the binding pose of arachidonic acid in this mutant structure was not stable. To further validate this viewpoint, we also estimated the binding free energies of the arachidonic acid in both wild-type and mutant CYP2J2 structures. The binding free energy of the arachidonic acid in the wild-type and T143A mutant CYP2J2 structure was about −40.71 (pK_i = 6.86), indicating that the T143A mutation had little influence on the arachidonic acid binding. The binding free energy of the arachidonic acid in the N404Y mutant CYP2J2 structure was ∼−34.84 kJ/mol (pK_i = 5.87), a little higher than that in the wild-type CYP2J2 structure. This observation indicated that the N404Y mutation could lower the binding affinity of the arachidonic acid.

CONCLUSION

As playing crucial roles in physiology and pathophysiology in inflammatory reactions, CYP2J2 and EETs have been implicated in the pathogenesis of coronary artery disease and hypertension. Some CYP2J2 polymorphisms can significantly reduce the enzyme activity. For instance, T143A exhibits only 59% of the wild-type enzyme activity; N404Y is essentially inactive in the arachidonic acid mechanism, showing only 5% of the wild-type enzyme activity. Lacking experimental structural data, the detailed mechanism for the mutation-induced dysfunction in the metabolism of arachidonic acid is still unclear. In the current study, structural models of the wild-type CYP2J2 and two mutants (T143A and N404Y) were predicted by molecular modeling. On the basis of the structural analysis of the computational models, a detailed mechanism was proposed to explain the mutation-induced dysfunction in the metabolism of arachidonic acid (Figure 6). The substitution of alanine for threonine at amino acid position 143 destabilized

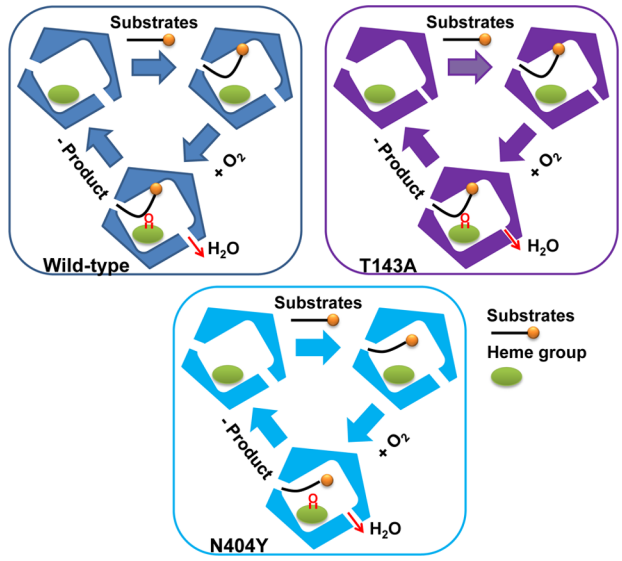

Figure 6. The proposed mechanism for the mutation-induced dysfunction in the metabolism of arachidonic acid. The T143A mutation could destabilize the C helix, further placing the water access channel in a closed state to prevent the escape of the produced water molecules during the catalytic processes; the N404Y mutation could reposition the side-chain of Leu^{378}, making it no longer form a hydrogen bond with the carboxyl group of arachidonic acid. This hydrogen bond was regarded to be essential for substrate recognition and positioning in a correct orientation.

the C helix, resulting in the water access channel adopting a closed state to prevent the escape of the produced water molecules during the catalytic processes. Although N404Y was far away from the active site pocket and not in the putative SRS sites, this mutation was able to reposition the side-chain of Leu^{378} by the steric effect of its large and aromatic side-chain, breaking down the hydrogen bond between Leu^{378} and the carboxyl group of arachidonic acid and weakening the substrate binding affinity and recognition ability. All these findings can provide an in-depth understanding of the arachidonic acid metabolism, giving useful indications for the treatment of coronary artery disease and hypertension as well as drug development.

ASSOCIATED CONTENT

Supporting Information

The chemical structure of arachidonic acid, the sequence alignment between CYP2J2 and its template structure, QMEAN scores, and the RMS deviations along the simulation trajectories. This material is available free of charge via the Internet at http://pubs.acs.org.

AUTHOR INFORMATION

Corresponding Author

*Tel.: (86) 21 3420-7344. Fax: (86) 21 3420-6059. E-mail: jfwang8113@sjtu.edu.cn (J.F.-W.), yxli@sibs.ac.cn (Y.X.-L.).

Present Addresses

‡College of Life Sciences and Biotehnology, Shanghai Jiao Tong Univesrity, Shanghai 200240, China

§Key Laboratory of Systems Biology, Shanghai Institutes for Biological Sciences, Chinese Academy of Sciences, Shanghai 200031, China

∥Shanghai Center for Bioinformation Technology, 1278 Keyuan Road, Shanghai 201203, China

Author Contributions

The manuscript was written through contributions of all authors. All authors have given approval to the final version of the manuscript.

Notes

The authors declare no competing financial interest.

■ ACKNOWLEDGMENTS

This work was supported by the grants from National Natural Science Foundation of China (No. 31200547), Doctoral Program Foundation of Institutions of Higher Education of China (No. 20110073120078), Scientific Research Foundation for the Returned Overseas Chinese Scholars, State Education Ministry (No. 10GJY205006), and the China Postdoctoral Science Foundation (No. 20110490068).

■ ABBREVIATIONS

ARA, arachidonic acid; CYP, Cytochrome P450; EET, epoxyeicosatrienoic acid; EDHF, endothelium-derived hyperpolarizing factor

■ REFERENCES

(1) Sprecher, H. Metabolism of highly unsaturated n-3 and n-6 fatty acids. *Biochim. Biophys. Acta* **2000**, *1486*, 219−231.
(2) MacDonald, J. I.; Sprecher, H. Phospholipid fatty acid remodeling in mammalian cells. *Biochim. Biophys. Acta* **1991**, *1084*, 105−121.
(3) Funk, C. D. Prostaglandins and leukotrienes: advances in eicosanoid biology. *Science* **2001**, *294*, 1871−1875.
(4) Harris, W. S.; Mozaffarian, D.; Rimm, E.; Kris-Etherton, P.; Rudel, L. L.; Appel, L. J.; Engler, M. M.; Engler, M. B.; Sacks, F. Omega-6 fatty acids and risk for cardiovascular disease: a science advisory from the American Heart Association Nutrition Subcommittee of the Council on Nutrition, Physical Activity, and Metabolism; Council on Cardiovascular Nursing; and Council on Epidemiology and Prevention. *Circulation* **2009**, *119*, 902−907.
(5) Ferrucci, L.; Cherubini, A.; Bandinelli, S.; Bartali, B.; Corsi, A.; Lauretani, F.; Martin, A.; Andres-Lacueva, C.; Senin, U.; Guralnik, J. M. Relationship of plasma polyunsaturated fatty acids to circulating inflammatory markers. *J. Clin. Endocrinol. Metab.* **2006**, *91*, 439−446.
(6) Zeldin, D. C. Epoxygenase pathways of arachidonic acid metabolism. *J. Biol. Chem.* **2001**, *276*, 36059−36062.
(7) Fleming, I. Vascular cytochrome p450 enzymes: physiology and pathophysiology. *Trends. Cardiovasc. Med.* **2008**, *18*, 20−25.
(8) Spector, A. A. Arachidonic acid cytochrome P450 epoxygenase pathway. *J. Lipid Res.* **2009**, *50*, S52−S56.
(9) Wang, H.; Lin, L.; Jiang, J.; Wang, Y.; Lu, Z. Y.; Bradbury, J. A.; Lih, F. B.; Wang, D. W.; Zeldin, D. C. Up-regulation of endothelial nitric-oxide synthase by endothelium-derived hyperpolarizing factor involves mitogen-activated protein kinase and protein kinase C signaling pathways. *J. Pharmacol. Exp. Ther.* **2003**, *307*, 753−764.
(10) Loot, A. E.; Popp, R.; Fisslthaler, B.; Vriens, J.; Nilius, B.; Fleming, I. Role of cytochrome P450-dependent transient receptor potential V4 activation in flow-induced vasodilatation. *Cardiovasc. Res.* **2008**, *80*, 445−452.
(11) Node, K.; Huo, Y.; Ruan, X.; Yang, B.; Spiecker, M.; Ley, K.; Zeldin, D. C.; Liao, J. K. Anti-inflammatory properties of cytochrome P450 epoxygenase-derived eicosanoids. *Science* **1999**, *285*, 1276−1279.
(12) Spiecker, M.; Liao, J. K. Vascular protective effects of cytochrome p450 epoxygenase-derived eicosanoids. *Arch. Biochem. Biophys.* **2005**, *433*, 413−420.
(13) Gainer, J. V.; Bellamine, A.; Dawson, E. P.; Womble, K. E.; Grant, S. W.; Wang, Y.; Cupples, L. A.; Guo, C. Y.; Demissie, S.; O'Donnell, C. J.; Brown, N. J.; Waterman, M. R.; Capdevila, J. H. Functional variant of CYP4A11 20-hydroxyeicosatetraenoic acid synthase is associated with essential hypertension. *Circulation* **2005**, *111*, 63−69.
(14) Imig, J. D.; Hammock, B. D. Soluble epoxide hydrolase as a therapeutic target for cardiovascular diseases. *Nat. Rev. Drug Discovery* **2009**, *8*, 794−805.
(15) Laffer, C. L.; Laniado-Schwartzman, M.; Wang, M. H.; Nasjletti, A.; Elijovich, F. Differential regulation of natriuresis by 20-hydroxyeicosatetraenoic Acid in human salt-sensitive versus salt-resistant hypertension. *Circulation* **2003**, *107*, 574−578.
(16) Wu, S.; Moomaw, C. R.; Tomer, K. B.; Falck, J. R.; Zeldin, D. C. Molecular cloning and expression of CYP2J2, a human cytochrome P450 arachidonic acid epoxygenase highly expressed in heart. *J. Biol. Chem.* **1996**, *271*, 3460−3468.
(17) Spiecker, M.; Darius, H.; Hankeln, T.; Soufi, M.; Sattler, A. M.; Schaefer, J. R.; Node, K.; Borgel, J.; Mugge, A.; Lindpaintner, K.; Huesing, A.; Maisch, B.; Zeldin, D. C.; Liao, J. K. Risk of coronary artery disease associated with polymorphism of the cytochrome P450 epoxygenase CYP2J2. *Circulation* **2004**, *110*, 2132−2136.
(18) King, L. M.; Ma, J.; Srettabunjong, S.; Graves, J.; Bradbury, J. A.; Li, L.; Spiecker, M.; Liao, J. K.; Mohrenweiser, H.; Zeldin, D. C. Cloning of CYP2J2 gene and identification of functional polymorphisms. *Mol. Pharmacol.* **2002**, *61*, 840−852.
(19) Strushkevich, N.; Usanov, S. A.; Plotnikov, A. N.; Jones, G.; Park, H. W. Structural analysis of CYP2R1 in complex with vitamin D3. *J. Mol. Biol.* **2008**, *380*, 95−106.
(20) Blundell, T. L.; Sibanda, B. L.; Sternberg, M. J.; Thornton, J. M. Knowledge-based prediction of protein structures and the design of novel molecules. *Nature* **1987**, *326*, 347−352.
(21) Jones, T. A.; Thirup, S. Using known substructures in protein model building and crystallography. *EMBO J.* **1986**, *5*, 819−822.
(22) Wang, J. F.; Wei, D. Q.; Lin, Y.; Wang, Y. H.; Du, H. L.; Li, Y. X.; Chou, K. C. Insights from modeling the 3D structure of NAD(P)H-dependent D-xylose reductase of Pichia stipitis and its binding interactions with NAD and NADP. *Biochem. Biophys. Res. Commun.* **2007**, *359*, 323−329.
(23) Wang, J. F.; Chou, K. C. Insights from studying the mutation-induced allostery in the M2 proton channel by molecular dynamics. *Protein Eng. Des. Sel.* **2010**, *23*, 663−666.
(24) Wang, J. F.; Chou, K. C. Insights from modeling the 3D structure of New Delhi metallo-beta-lactamse and its binding interactions with antibiotic drugs. *PLoS One* **2011**, *6*, e18414.
(25) Wang, J. F.; Wei, D. Q.; Li, L.; Zheng, S. Y.; Li, Y. X.; Chou, K. C. 3D structure modeling of cytochrome P450 2C19 and its implication for personalized drug design. *Biochem. Biophys. Res. Commun.* **2007**, *355*, 513−519.
(26) Wang, J. F.; Wei, D. Q.; Chen, C.; Li, Y.; Chou, K. C. Molecular modeling of two CYP2C19 SNPs and its implications for personalized drug design. *Protein Pept. Lett.* **2008**, *15*, 27−32.
(27) Wang, J. F.; Wei, D. Q.; Chou, K. C. Drug candidates from traditional Chinese medicines. *Curr. Top. Med. Chem.* **2008**, *8*, 1656−1665.
(28) Wang, J. F.; Wei, D. Q.; Chou, K. C. Pharmacogenomics and personalized use of drugs. *Curr. Top. Med. Chem.* **2008**, *8*, 1573−1579.
(29) Wu, S.; Skolnick, J.; Zhang, Y. Ab initio modeling of small proteins by iterative TASSER simulations. *BMC Biol.* **2007**, *5*, 17.
(30) Labute, P. The generalized Born/volume integral implicit solvent model: estimation of the free energy of hydration using London dispersion instead of atomic surface area. *J. Comput. Chem.* **2008**, *29*, 1693−1698.
(31) Rocchia, W.; Alexov, E.; Honing, B. Extending the applicability of the nonlinear Poisson-Boltzmann equation: multiple dielectric constants and multivalent ions. *J. Phys. Chem. B* **2001**, *105*, 6507−6514.
(32) Ponder, J. W.; Case, D. A. Force fields for protein simulations. *Adv. Protein Chem.* **2003**, *66*, 27−85.
(33) Schoneboom, J. C.; Lin, H.; Reuter, N.; Thiel, W.; Cohen, S.; Ogliaro, F.; Shaik, S. The elusive oxidant species of cytochrome P450 enzymes: characterization by combined quantum mechanical/molecular mechanical (QM/MM) calculations. *J. Am. Chem. Soc.* **2002**, *124*, 8142−8151.

(34) Case, D. A.; Cheatham, T. E., 3rd; Darden, T.; Gohlke, H.; Luo, R.; Merz, K. M., Jr.; Onufriev, A.; Simmerling, C.; Wang, B.; Woods, R. J. The Amber biomolecular simulation programs. *J. Comput. Chem.* **2005**, *26*, 1668−1688.
(35) Berendsen, H. J. C.; Postma, J. P. M.; van Gunsteren, W. F.; DiNola, A.; Haak, J. R. Molecular dynamics with coupling to an external bath. *J. Chem. Phys.* **1984**, *81*, 3684−3690.
(36) Lian, P.; Wei, D. Q.; Wang, J. F.; Chou, K. C. An allosteric mechanism inferred from molecular dynamics simulations on phospholamban pentamer in lipid membranes. *PLoS One* **2011**, *6*, e18587.
(37) Wang, Y.; Wei, D. Q.; Wang, J. F. Molecular dynamics studies on T1 lipase: insight into a double-flap mechanism. *J. Chem. Inf. Model.* **2010**, *50*, 875−878.
(38) Wang, Y.; Wu, X. L.; Wei, D. Q.; Li, Y. X.; Wang, J. F. Autoinhibitory mechanism for the mutation-induced impaired FGF9 signaling. *J. Chem. Inf. Model.* **2012**, *52*, 2422−2429.
(39) Wang, Y. J.; Wang, J. F.; Ping, J.; Yu, Y.; Wang, Y.; Lian, P.; Li, X.; Li, Y. X.; Hao, P. Computational studies on the substrate interactions of influenza A virus PB2 subunit. *PLoS One* **2012**, *7*, e44079.
(40) Perdih, A.; Bren, U.; Solmajer, T. Binding free energy calculations of N-sulphonyl-glutamic acid inhibitors of MurD ligase. *J. Mol. Model.* **2009**, *15*, 983−996.
(41) Bren, U.; Janežič, D. Individual degrees of freedom and the salvation properties of water. *J. Chem. Phys.* **2012**, *137*, 024108.
(42) Wang, R.; Lai, L.; Wang, S. Further development and validation of empirical scoring functions for structure-based binding affinity prediction. *J. Comput.-Aided Mol. Des.* **2002**, *16*, 11−26.
(43) Wang, J. F.; Zhang, C. C.; Chou, K. C.; Wei, D. Q. Structure of cytochrome p450s and personalized drug. *Curr. Med. Chem.* **2009**, *16*, 232−244.
(44) Li, J.; Wei, D. Q.; Wang, J. F.; Li, Y. X. A negative cooperativity mechanism of human CYP2E1 inferred from molecular dynamics simulations and free energy calculations. *J. Chem. Inf. Model.* **2011**, *51*, 3217−3225.
(45) Ping, J.; Wang, Y. J.; Wang, J. F.; Li, X.; Li, Y. X.; Hao, P. Negatively cooperative binding properties of human cytochrome P450 2E1 with monocyclic substrates. *Curr. Drug Metab.* **2012**, *13*, 1024−1031.
(46) Bren, U.; Oostenbrink, C. Cytochrome P450 3A4 inhibition by ketoconazole: trackling the problem of ligand cooperativity using molecular dynamics simulations and free-energy calculations. *J. Chem. Inf. Model* **2012**, *52*, 1573−1582.
(47) Imai, M.; Shimada, H.; Watanabe, Y.; Matsushima-Hibiya, Y.; Makino, R.; Koga, H.; Horiuchi, T.; Ishimura, Y. Uncoupling of the cytochrome P-450cam monooxygenase reaction by a single mutation, threonine-252 to alanine or valine: possible role of the hydroxy amino acid in oxygen activation. *Proc. Natl. Acad. Sci. U.S.A.* **1989**, *86*, 7823−7827.
(48) Wang, J. F.; Chou, K. C. Molecular modeling of cytochrome P450 and drug metabolism. *Curr. Drug Metab.* **2010**, *11*, 342−346.
(49) Wu, S.; Zhang, Y. LOMETS: a local meta-threading-server for protein structure prediction. *Nucleic Acids Res.* **2007**, *35*, 3375−3382.
(50) Laskowski, R. A.; Moss, D. S.; Thornton, J. M. Main-chain bond lengths and bond angles in protein structures. *J. Mol. Biol.* **1993**, *231*, 1049−1067.
(51) Benkert, P.; Tosatto, S. C.; Schomburg, D. QMEAN: A comprehensive scoring function for model quality assessment. *Proteins* **2008**, *71*, 261−277.
(52) Colovos, C.; Yeates, T. O. Verification of protein structures: patterns of nonbonded atomic interactions. *Protein Sci.* **1993**, *2*, 1511−1519.
(53) Luthy, R.; Bowie, J. U.; Eisenberg, D. Assessment of protein models with three-dimensional profiles. *Nature* **1992**, *356*, 83−85.
(54) Gotoh, O. Substrate recognition sites in cytochrome P450 family 2 (CYP2) proteins inferred from comparative analyses of amino acid and coding nucleotide sequences. *J. Biol. Chem.* **1992**, *267*, 83−90.
(55) Meunier, B.; de Visser, S. P.; Shaik, S. Mechanism of oxidation reactions catalyzed by cytochrome p450 enzymes. *Chem. Rev.* **2004**, *104*, 3947−3980.
(56) Chen, Q.; Zhang, T.; Wang, J. F.; Wei, D. Q. Advances in human cytochrome p450 and personalized medicine. *Curr. Drug Metab.* **2011**, *12*, 436−444.
(57) Gonzalez-Diaz, H.; Prado-Prado, F.; Garcia-Mera, X.; Alonso, N.; Abeijon, P.; Caamano, O.; Yanez, M.; Munteanu, C. R.; Pazos, A.; Dea-Ayuela, M. A.; Gomez-Munoz, M. T.; Garijo, M. M.; Sansano, J.; Ubeira, F. M. MIND-BEST: Web Server for Drugs and Target Discovery; Design, Synthesis, and Assay of MAO-B Inhibitors and Theoretical-Experimental Study of G3PDH Protein from Trichomonas gallinae. *J. Proteome Res.* **2011**, *10*, 1698−1718.
(58) Gonzalez-Diaz, H.; Prado-Prado, F.; Sobarzo-Sanchez, E.; Haddad, M.; Chevalley, S. M.; Valentin, A.; Quetin-Leclercq, J.; Dea-Ayuela, M. A.; Teresa Gomez-Munos, M.; Munteanu, C. R.; Jose Torres-Labandeira, J.; Garcia-Mera, X.; Tapia, R. A.; Ubeira, F. M. NL MIND-BEST: A web server for ligands and proteins discovery-Theoretic-experimental study of proteins of Giardia lamblia and new compounds active against Plasmodium falciparum. *J. Theor. Biol.* **2011**, *276*, 229−249.
(59) González-Díaz, H.; Vilar, S.; Santana, L.; Uriarte, E. Medicinal Chemistry and Bioinformatics − Current Trends in Drugs Discovery with Networks Topological Indices. *Curr. Top. Med. Chem.* **2007**, *7*, 1025−39.
(60) González-Díaz, H.; González-Díaz, Y.; Santana, L.; Ubeira, F. M.; Uriarte, E. Proteomics, networks and connectivity indices. *Proteomics* **2008**, *8*, 750−778.